Structural Determinants of the Catalytic Ni_a-L Intermediate of [NiFe]-Hydrogenase

Armel F. T. Waffo[a], Christian Lorent[a], Sagie Katz[a], Janna Schoknecht[a], Oliver Lenz[a], Ingo Zebger[a*] and Giorgio Caserta[a*]

[a]Institut für Chemie, Technische Universität Berlin, Straße des 17. Juni 135, 10623 Berlin, Germany

*Emails: giorgio.caserta@tu-berlin.de, ingo.zebger@tu-berlin.de

Keywords: metalloenzyme, hydrogenase, catalytic cycle, spectroscopy

Abstract

[NiFe]-hydrogenases catalyze the reversible cleavage of H_2 into two protons and two electrons at the inorganic heterobimetallic NiFe center of the enzyme. Their catalytic cycle involves at least four intermediates, some of which are still under debate. While the core reaction, including H_2/H^- binding, takes place at the inorganic cofactor, a major challenge lies in identifying those amino acid residues that contribute to the reactivity and how they stabilize (short-lived) intermediate states. Using cryogenic infrared and electron paramagnetic resonance spectroscopy on the regulatory [NiFe]-hydrogenase from *Cupriavidus necator*, a model enzyme for the analysis of catalytic intermediates, we deciphered the structural basis of the hitherto elusive Ni_a-L intermediates. We unveiled the protonation states of a proton-accepting glutamate and a Ni-bound cysteine residue in the Ni_a-L1, Ni_a-L2, and the hydride-binding Ni_a-C intermediates, as well as previously unknown conformational changes of amino acid residues in proximity of the bimetallic active site. As such, this study unravels the complexity of the Ni_a-L intermediate and reveals the importance of the protein scaffold in fine-tuning proton and electron dynamics in [NiFe]-hydrogenase.

1. Introduction

By making use of the transition metals nickel and iron, [NiFe]-hydrogenases catalyze the reversible reaction $H_2 \rightleftarrows 2H^+ + 2e^-$ with high efficiency under ambient conditions.[1,2] Catalysis takes place at the unique NiFe center, and the electrons are channeled through a series of Fe–S clusters, which vary in number and composition.[1,3] The NiFe active site is anchored to the protein scaffold via two cysteines bound terminally to Ni and two cysteines with bridging bonds between Ni and Fe. The Fe is additionally ligated by one CO and two CN^- (strong-field) ligands, which stabilize a low-spin Fe^{II} configuration (**Fig. 1**).[4,5] Infrared (IR) spectroscopy has played a pivotal role in characterizing the various active and

inhibited states of hydrogenases, observing shifts in the vibrational bands of the active site CO and CN^- ligands due to structural and redox changes.[6] Recent achievements in this regard have been summarized elsewhere.[7–9] The O_2-tolerant regulatory [NiFe]-hydrogenase (RH) from the 'Knallgas' bacterium *Cupriavidus necator* (*Cn*) has been used as model enzyme to elucidate the electronic and molecular structure of certain catalytic intermediates. Among them, the Ni_a-S ($Ni^{II}Fe^{II}$) and the Ni_a-C (Ni^{III}-H-Fe^{II}) intermediates (see **Fig. 1** for structural details) can be enriched almost stoichiometrically in RH and have been investigated using a plethora of spectroscopic techniques, including IR, electronic paramagnetic resonance (EPR), Mössbauer, resonance Raman (RR), and nuclear resonance vibrational spectroscopy (NRVS).[10–15] While there is consensus on the structures of Ni_a-C and Ni_a-S, those of Ni_a-SR (Ni^{II}-H-Fe^{II}) and Ni_a-L are still highly debated as both comprise various sub-forms.[7,16,17] These are tentatively assigned to active site states with identical electronic configurations, but differing in proton localization. For instance, Ni_a-L represents a tautomeric form of Ni_a-C in which electrons from the hydride are stored on the nickel yielding a formal Ni^I species, while the resulting proton may be bound to different amino acid residues depending on the nature of the sub-state (**Fig. 1**). The Ni_a-L intermediate has been first observed for the [NiFe]-hydrogenase *Allochromatium vinosum* (formerly *Chromatium vinosum*) in 1985,[18] however, convincing evidence of its catalytic relevance was not provided until three decades later by complementary investigations on the O_2-sensitive [NiFe]-hydrogenase from *Desulfovibrio vulgaris* Miyazaki F (*Dv*MF), the O_2-tolerant membrane-bound [NiFe]-hydrogenase Hyd1 from *Escherichia coli* (*Ec*Hyd1) and the soluble [NiFe]-hydrogenase from *Pyrococcus furiosus* (*Pf*SHI).[19–21] Different Ni_a-L sub-forms have been identified for all three enzymes. Although the way these species have been classified/named is not always consistent, three main species (i.e., Ni_a-L1, Ni_a-L2 and Ni_a-L3) have been described and insights from experimental and theoretical works point toward the protonation of one of the Ni-bound terminal cysteines in some of these states.[7,16]

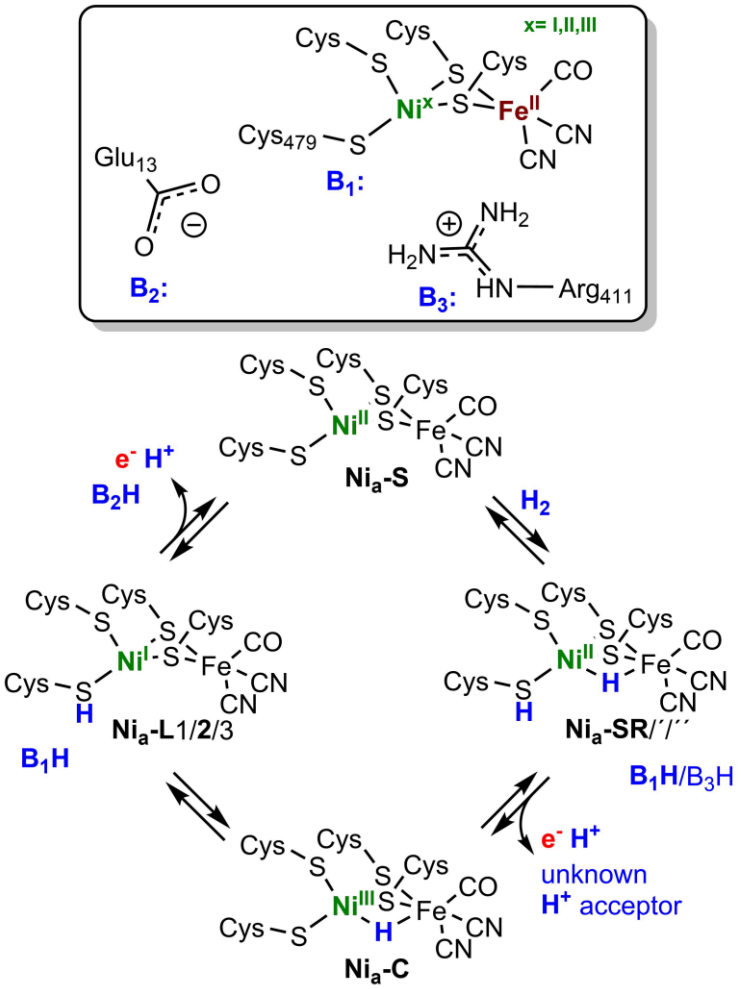

Figure 1. Schematic representation of the active site of [NiFe]-hydrogenases (top) and the proposed catalytic mechanism involving the intermediates Ni_a-S, Ni_a-SR, Ni_a-C and Ni_a-L (bottom). During catalysis, only nickel is redox-active, while the iron maintains an Fe^{II} low-spin configuration throughout the catalytic cycle. Ni_a-SR and Ni_a-L intermediates comprise three sub-forms, two of which (Ni_a-L2 and Ni_a-SR, bold) have been extensively characterized.[7,16] The proposed proton acceptors in the vicinity of the active site are a Ni-bound terminal cysteine (Cys479 in *Cn*RH, B_1), a nearby glutamate (Glu13 in *Cn*RH, B_2) and an arginine (Arg411 in *Cn*RH, B_3), which are displayed in the top panel in their protonated/deprotonated forms according to physiological conditions.

Changes in the protonation state of a Ni-bound Cys (corresponding to Cys479 in *Cn*RH **Fig. S1**) of the O_2-sensitive *Dv*MF [NiFe]-hydrogenase have been shown by cryogenic IR investigations of the photoinduced transition from Ni_a-C to Ni_a-L2,[22] an ultra-high resolution structure of the enzyme in the Ni_a-SR state (85 % Ni_a-SR) and a combined DFT/NRVS study of the Ni_a-SR species.[23,24] Conversely, IR spectroscopic experiments performed on the O_2-tolerant *Ec*Hyd1 revealed no change in the protonation state of the corresponding cysteine (Cys576 in *Ec*Hyd1, **Fig. S1**) in any of the Ni_a-S, Ni_a-C, Ni_a-L2/3, or Ni_a-SR´/´´ states.[25] This discrepancy suggests that different proton acceptors might coexist in [NiFe]-hydrogenases, with some reports speculating that such diversity might be related to the O_2-tolerance/sensitivity of hydrogenases.[26]

Herein, we employed cryogenic IR and EPR to resolve the longstanding debate about the structure of the Ni_a-L1 and Ni_a-L2 sub-forms, using *Cn*RH as model hydrogenase. With this approach we showed that in both Ni_a-L1 and Ni_a-L2 sub-forms a proton is localized at a nearby cysteine thiolate, which forms a hydrogen bond with the proton-accepting glutamate (Glu13 in *Cn*RH, **Fig. 1**) in the Ni_a-L2 intermediate. We also uncovered the protonation state of residues in the second coordination sphere as well as previously unknown conformational changes of amino acids in proximity of the bimetallic active site. This allowed us to define new structural determinants of the active site in catalytic intermediates.

Results and Discussion

Ni_a-C to Ni_a-L photoreaction

The active site of as-isolated (oxidized) *Cn*RH resides in the diamagnetic Ni_a-S state, which is characterized at 90 K by an absorption at 1946 cm^{-1} related to the ν_{CO} stretching vibration and two bands at 2073 cm^{-1} and 2082 cm^{-1} deriving from the symmetric and asymmetric ν_{CN} stretching modes, respectively (**Fig. 2a**, green trace, **Table S1**).[2,27] The Ni_a-S intermediate is stable over a wide pH and temperature range.[28,29] Reduction of as-isolated *Cn*RH with H_2 leads to an almost stoichiometric enrichment of the Ni_a-C intermediate, characterized by a ν_{CO} at 1964 cm^{-1} and ν_{CN} stretches at 2071 cm^{-1} and 2085 cm^{-1} (**Fig. 2a**, blue trace, **Table S1**). A small Ni_a-SR population (ν_{CO} at 1948 cm^{-1}) was detectable at 298 K (**Fig. S2**) but virtually absent at 90 K (**Fig. 2a**), suggesting the presence of a thermal equilibrium between the two reduced species that shifts toward Ni_a-C at lower temperatures (**Fig. 2a**).

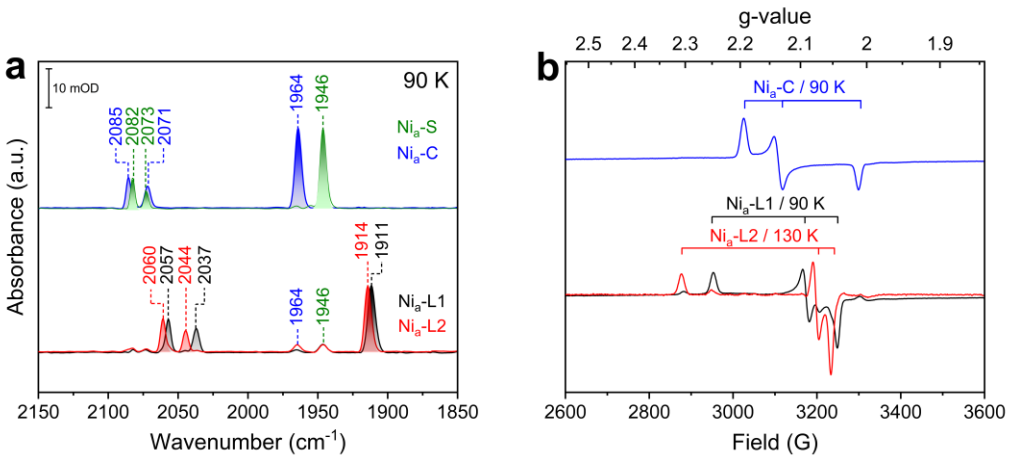

Figure 2. IR (**a**) and EPR (**b**) spectra of *Cn*RH in various redox states. The IR spectrum of the as-isolated *Cn*RH is dominated by absorptions that are attributed to the diamagnetic Ni_a-S state (green trace and labels) whereas the H_2-reduced *Cn*RH exhibits predominantly bands of the paramagnetic Ni_a-C intermediate (blue), as confirmed by the corresponding EPR data (blue trace in **b**). The IR spectrum depicted in black represents the light-induced Ni_a-L1 state obtained after illumination of H_2 reduced *Cn*RH sample with an LED array at 460 nm. Keeping the protein sample at a higher temperature (T > 120 K) in darkness, the Ni_a-L1 species converts completely to the Ni_a-L2 state (depicted in red). The EPR spectrum obtained during illumination at 90

K exhibits mainly signals of the Ni_a-L1 species,[10] which converts almost stoichiometrically to Ni_a-L2 at higher temperatures (130 K). The ν_{CO} and ν_{CN} bands related to the CO and CN stretching vibrations of the diatomic active site ligands are labelled with their corresponding wavenumbers in the IR spectra.

Ni_a-C has been shown to photoconvert into Ni_a-L species in several [NiFe]-hydrogenases,[2,16] but the latter intermediate was detected almost exclusively at cryogenic temperatures due to the rapid Ni_a-L to Ni_a-C back-conversion.[2,10,18] However, in a few studies, CO and CN absorptions associated to Ni_a-L intermediates have been observed also at ambient temperature. Examples are i) time-resolved and steady state IR spectroscopic studies on *Pf*SH1 hydrogenase and its R355K variant,[17,21,30] ii) spectroelectrochemical and pH-dependent studies on *Ec*Hyd1 protein solutions and single crystals,[20,25,26,31] and iii) IR studies on isolated *C. necator* hydrogenase large subunits treated with reducing agents.[5,28]

Irradiation of RH samples enriched in the Ni_a-C state at 90 K (pH 8.0) with an LED array (460 nm) results in the enrichment of a single species, Ni_a-L1, characterized by a ν_{CO} band at 1911 cm^{-1} and ν_{CN} stretches at 2037 and 2056 cm^{-1} (black trace in **Fig. 2a**, **Table S1**). These signals appear in the spectral range of the previously observed Ni_a-L1 and Ni_a-L2 species of *Pf*SH1.[21,32] When the temperature was first increased (T> 120K) and then decreased back to 90 K, we observed the formation of a second species, Ni_a-L2, in the dark, with a ν_{CO} at 1914 cm^{-1} and ν_{CN} at 2044 and 2061 cm^{-1} (red trace in **Fig. 2a**, **Table S1**). To our knowledge, this is the first report of an homogenous preparation of both Ni_a-L1 and Ni_a-L2 species, enabling IR difference spectroscopy for a detailed structural analysis (see below).[16] Ni_a-L1 converts to Ni_a-L2 (**Fig. S3a, b**), and the rate of the conversion accelerated at higher temperatures (T > 120 K) in agreement with the temperature-dependent EPR data recorded for the Ni_a-L1 to Ni_a-L2 conversions of *Desulfovibrio gigas* and *Desulfovibrio fructosivorans* (often incorrectly called *D. fructosovorans*[33]) hydrogenases.[34,35] To confirm that the herein observed IR species (ν_{CO} at 1911 and 1914 cm^{-1}) represent the previously EPR-detected Ni_a-L1/2 states of *Cn*RH,[10] we recorded the EPR spectra of H_2-reduced enzyme with and without illumination (**Fig. 2b**). In the dark, the typical rhombic signal of Ni_a-C (g_x = 2.193, g_y = 2.136 g_z = 2.013, **Table S2**) was observed. Continuous illumination of the H_2-reduced enzyme led to the formation of two EPR-active states exhibiting the previously observed spectral signatures of Ni_a-L1 (g_x = 2.248, g_y = 2.090, g_z = 2.044, **Table S2**) and Ni_a-L2 (g_x = 2.307, g_y = 2.075, g_z = 2.052, **Table S2**).[10] In line with the IR data, the Ni_a-L2 state is most prominent at higher temperatures (T > 120 K), while Ni_a-L1 dominates at lower temperatures (**Fig. S4a-j**). In addition, power-dependent saturation experiments of the Ni_a-C- and Ni_a-L2-related EPR signals suggest a dipolar interaction of the paramagnetic catalytic center with the reduced [4Fe-4S] cluster in proximal position (**Fig. S5**). In agreement with the IR data, the Ni_a-L1 to Ni_a-L2 transformation was also observed by EPR in the dark (**Fig. S6**).

Remarkably, our cryogenic IR data indicate no reversion of Ni_a-L2 to Ni_a-L1, either when the temperature was set back to 90 K after enrichment of Ni_a-L2 (**Fig. S7a**) or raised at higher temperatures (T > 130 K), where only conversion of the Ni_a-L1 to Ni_a-L2 and Ni_a-L2 to Ni_a-C was observed (**Fig. S7b**). We also recorded IR spectra for the sequence of Ni_a-C → Ni_a-L1 → Ni_a-L2 transformations at pH 6.0 and 7.0 (**Fig. S8a**, **b**), which did not indicate any pH effect on the sequential order of transformations. In summary, our data on the isolated Ni_a-L1 and Ni_a-L2 species rule out both a temperature- and pH-dependent equilibrium between these sub-forms suggesting that Ni_a-L1 occurs solely as a transient species that spontaneously transforms into the more stable Ni_a-L2 species.

Structural details of the Ni_a-L1 and Ni_a-L2 sub-forms of the [NiFe] active site

While hydrogenases are usually investigated by IR (absorption) spectroscopy with the aim to monitor different redox states via the inherent stretching vibrations of the CO and CN ligands of the active site, we applied herein difference spectroscopy to study structural changes at amino acids in the first and second coordination spheres of the $NiFe(CN)_2(CO)$ cofactor.[36–38] Upon illumination of *Cn*RH in the Ni_a-C state at 90 K, the light-*minus*-dark IR difference spectrum (Ni_a-C-*minus*-Ni_a-L1) shows prominent positive CO and CN absorptions related to the Ni_a-L1 that are centered at 1911, 2037, and 2056 cm^{-1}, while negative bands belonging to the Ni_a-C species are found at-1964, 2071, and 2085 cm^{-1} (**Fig. 3a**, black trace). Strikingly, a small positive band was detected at ca 2548 cm^{-1} (**Fig. 3b**) that falls within the range of ν_{SH} stretching frequencies, suggesting protonation of a nearby cysteine thiolate in the Ni_a-L1 state.[37] This assumption is substantiated by complementary experiments with an enzyme sample prepared with D_2 and D_2O, which revealed a positive band at 1853 cm^{-1} (**Fig. 3c**, grey trace) that was absent in the H_2/H_2O-prepared enzyme (**Fig. 3c**, black trace) and thus assignable to a ν_{SD} mode.

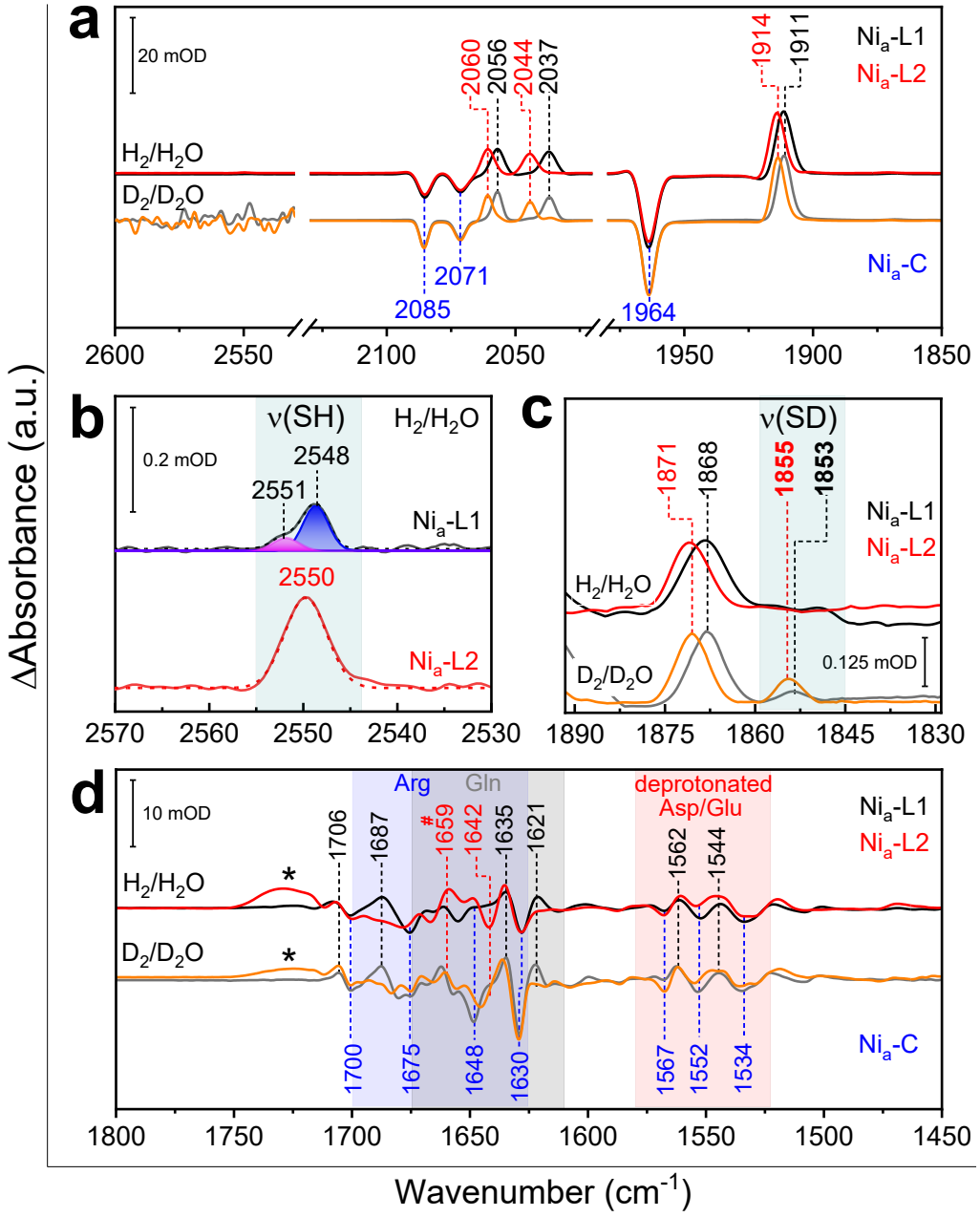

Figure 3. Light-*minus*-dark IR difference spectra of reduced *Cn*RH displaying negative absorption bands for Ni_a-C and positive signals for Ni_a-L1 and Ni_a-L2 species. (**a**) Spectral region comprising the absorptions related to the ν_{CO} and ν_{CN} stretching vibrations of the hydrogenase diatomic ligands as well as bands deriving from the ν_{SH} (**b**) and ν_{SD} (**c**) stretching modes of the protonated/deuterated Ni-bound cysteine. Difference spectra of *Cn*RH samples prepared with H_2/H_2O are shown in black and red, while the gray and orange traces show the spectra of the D_2/D_2O-prepared enzyme, respectively. Relevant vibrational bands are labelled with the corresponding wavenumbers. Panel (**d**) displays the corresponding frequency regime between 1800-1450 cm^{-1} of the light-*minus*-dark spectra. Spectral regions presumably containing contributions of arginine (blue), glutamine (grey), and deprotonated aspartate/glutamate (red) residues are highlighted. This spectral region may contain contributions from amide I and II absorptions, which occur between 1600-1700 cm^{-1} and 1510-1580 cm^{-1}, and are characteristic for changes in secondary structural elements.[39] The band marked with # most likely originates from OH bending vibrations of water molecules(s) in the proximity of the active site in the Ni_a-L2 state, which is supported by its disappearance in the spectra of D_2/D_2O-prepared enzymes. We consider the broad band around 1700-1730 cm^{-1} (marked with *) to be an artifact due to slight temperature fluctuations over time.

The observed H/D isotopic shift of 695 cm^{-1} between the ν_{SH} and ν_{SD} bands is consistent with previous observations on a protonated cysteine thiolate of *Dv*MF hydrogenase in the Ni_a-L2 state.[16,22] Here we show for the first time the protonation of a cysteine thiolate for the Ni_a-L1 intermediate. Considering previous spectroscopic and structural data on the *Dv*MF hydrogenase,[22,23] we propose that the sulfur atom of Cys479 in *Cn*RH serves as the acceptor of the proton released upon photolysis of the bridging hydride of the Ni_a-C state. After complete conversion to the Ni_a-L2 state, the respective Ni_a-L2-*minus*-Ni_a-C IR difference spectrum was calculated (**Fig. 3a**, red trace). Positive CO/CN bands were detected at 1914, 2044 and 2060 cm^{-1}, with the negative bands related to the Ni_a-C state remaining unchanged compared to the Ni_a-L1-*minus*-Ni_a-C difference spectrum. As with Ni_a-L1, positive ν_{SH}- and ν_{SD}-related bands were observed at 2550 cm^{-1} (for the H_2/H_2O sample) and 1855 cm^{-1} (for the D_2/D_2O sample), indicating that a protonated terminal cysteine is also present in the Ni_a-L2 intermediate (**Fig. 3b** and **3c**). Likewise, we observed an identical H/D isotopic shift of 695 cm^{-1} between the ν_{SH} and ν_{SD} vibrations for Ni_a-L2. Moreover, the ν_{SH} bands in Ni_a-L1 and Ni_a-L2 exhibit higher intensities than the corresponding ν_{SD} bands, which is consistent with the lower dipole moment of the S-D group compared to the S-H group[37] and confirms the overall assignment. Remarkably, the $\nu_{SH/D}$ bands in the Ni_a-L2 state are sharper and more intense than those detected in Ni_a-L1. Consistent with recent data on the ν_{SH} bands in pyruvate oxidase[40] as well as in hemoglobin and bacteriorhodopsin,[41,42] we correlate the higher integrated absorption coefficient for the $\nu_{SH/D}$ in Ni_a-L2 with a stronger polarization of the S-H/D bond of the protonated Cys479 due to hydrogen (H)-bonding (see below). The broader ν_{SH} and ν_{SD} absorptions observed for the Ni_a-L1 state might therefore be based on a mixture of rotamers of protonated Cys479 (see subcomponent bands in **Fig. 3b**).[43,44]

In the spectral region of ν_{SD} modes we also observed positive bands at 1868 (Ni_a-L1-*minus*-Ni_a-C spectrum) and 1871 cm^{-1} (Ni_a-L2-*minus*-Ni_a-C) that are insensitive to the H/D isotope shift. As they display an identical temperature dependence as the ν_{CO} band in the Ni_a-L1 and Ni_a-L2 species (**Fig. 3c**), we assign these minor signals to the ν_{CO} bands of the Ni_a-L1 and Ni_a-L2 species originating from ^{13}CO ligands (natural abundance of ^{13}C: 1.1 %). Indeed, the observed $\Delta\nu_{CO}$ isotope shift of 44 cm^{-1} (e.g., Ni_a-L2 with ν_{CO} bands at 1914 and 1871 cm^{-1}, **Fig. 3a,c**) is identical to that previously measured for the Ni_a-S intermediate of RH (1943 cm^{-1} and 1899 cm^{-1} for CO and ^{13}CO, respectively).[45] It should be emphasized that the observation of these low-intensity bands is an indication of a very high signal-*to*-noise ratio in the IR difference spectra, which allowed us to detect the previously postulated ν_{SH} and ν_{SD} features in Ni_a-L1 as well as additional features in the frequency regime between 1800 and 1450 cm^{-1} (**Fig. 3d**, see below).

A recent work on the Ni_a-C to Ni_a-L2 photo-transformation in the *Dv*MF hydrogenase revealed positive and negative C=O stretching frequencies of Ni_a-L2 and Ni_a-C at 1700 and 1727 cm^{-1}, respectively, which

shifted to lower frequencies of 1683 and 1715 cm^{-1} in a D_2/D_2O-treated sample.[8,22] These absorptions were assigned to stretching frequencies of the carboxylic group (ν_{COOH}) of a conserved glutamate (Glu13 in *Cn*RH), which are presumably involved in the formation of two hydrogen bonds in the Ni_a-L2 state (no protonated cysteine thiolate is involved) and a single hydrogen bond in the Ni_a-C state. Ni_a-L1/2-*minus*-Ni_a-C IR difference spectra of *Cn*RH showed several bands between 1700 and 1625 cm^{-1} and 1575 and 1500 cm^{-1}, but no H/D-sensitive signals between 1700 cm^{-1} and 1780 cm^{-1}, which would unambiguously support a protonation of the glutamate in the Ni_a-C and Ni_a-L1/2 states (**Fig. 3d**). Furthermore, most of the bands in this frequency region exhibit little to no change upon H/D labelling and appear in regions where deprotonated aspartate/glutamate (red), glutamine and asparagine (grey), arginine (blue), amide I/II, and water molecules exhibit distinct spectral contributions.[37] Based on a sequence alignment of *Cn*RH with [NiFe]-hydrogenases of known structures (**Fig. S1**), we identified the conserved Asp102, Glu13, Arg411, and Gln67 (present only in regulatory [NiFe]-hydrogenases and replaced by a His in standard [NiFe-hydrogenases)[46] that should be within 6 Å from the $NiFe(CN)_2(CO)$ site and therefore might contribute to the observed IR bands. To visualize the localization of the above amino acids, we used the predicted structural model of the RH large subunit HoxC in its apo form from the AlphaFold protein structure database[47] (**Fig. S9a**) and we fed this model into the AlphaFill algorithm[48], which implements ligands/cofactors/metals from experimentally determined structures into predicted apo-protein models to obtain a model of the holo-protein. The $NiFe(CN)_2(CO)$ binding site including the above amino acid residues of the resulting HoxC model is shown in **Fig. 4** (**Fig. S9b-c** shows the entire model of holo-HoxC and its overlay with the model of the apo-form). The AlphaFill model predicts a salt bridge between Arg411 and Asp102 (**Fig. 4b**), which has been experimentally determined in both O_2-tolerant and O_2-sensitive [NiFe]-hydrogenases.[23,49] Correspondingly, the positive and negative bands at 1687 and 1675 cm^{-1} (**Fig. 3b**) fall within the spectral range for the $\nu_{as}(CN_3H_5^+)$ of protonated arginine residues (Arg411 in *Cn*RH) interacting with negatively charged residues (glutamate/aspartate). Thus, the presence of several bands in the shown frequency regime of the Ni_a-L1/2-*minus*-Ni_a-C difference spectra indicates structural rearrangements of amino acid residues around the active site beyond the conserved Glu13 residue (see below).[22]

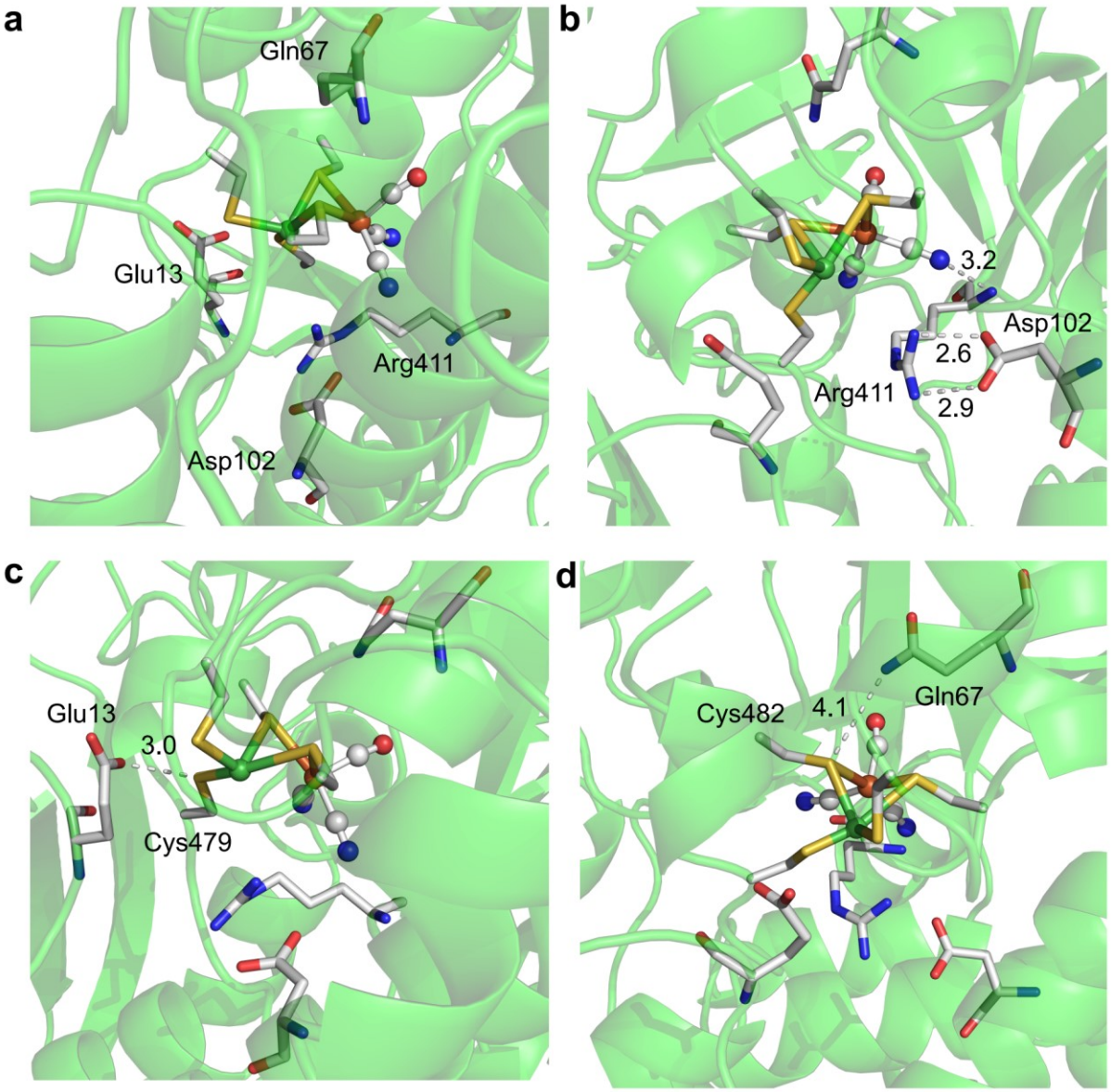

Figure 4. AlphaFill-predicted model of the *Cn*RH large subunit HoxC including the NiFe(CN)$_2$(CO) cofactor. (**a**) Active site region including the relevant residues Glu13, Gln67, Arg411, and Asp102. (**b**) Active site region showing a salt bridge (dashed) between Arg411 and Asp102 and a hydrogen bond between the peptide amino group of Arg411 and one CN ligand. (**c**) Active site region showing that Glu13 and Cys479 are in hydrogen bonding distance. (**d**) Active site region showing that the side-chain amino group of Gln67 points towards the bridging Cys482, as previously proposed.[50] The NiFe(CN)$_2$(CO) cofactor is shown in ball and stick representation. The coordinating cysteines (Cys60, 63, 479, and 482) and the relevant Glu13, Gln67, Arg411, and Asp102 residues are shown in stick representation. Color code: C, grey; O, red; N, blue; S, yellow; Ni, green; Fe, brown. The protein backbone is shown in cartoon representation (green). The entire model of HoxC is shown in **Fig. S9**.

Conformational changes of amino acid residues in proximity of the [NiFe] active site caused by the Ni_a-L1 to Ni_a-L2 conversion

Further details of on the two intermediates were obtained by calculating the energy barrier of the Ni_a-L1 to Ni_a-L2 transition based on the rate constants of the conversion determined at various

temperatures. Surprisingly, the integrals of the CO and CN bands that were evaluated as a function of time showed a bi-exponential behavior, indicating that two independent processes contribute to the Ni_a-L1 to Ni_a-L2 conversion. The E_a calculations for the two processes yielded values of 20.7 kJ mol^{-1} and 24.6 kJ mol^{-1}, respectively (**Fig. 5** and **Fig. S10,** see **Table S3** for fitting parameters). For comparison, the kinetic analysis of the Ni_a-L2 to Ni_a-C back-conversion (T > 180 K) revealed that the rebinding of the bridging hydride is a first-order process with an estimated E_a of 52.4 kJ mol^{-1}, which is consistent with previous results on *Dv*MF hydrogenase (**Fig. S11**, **Table S4**).[51]

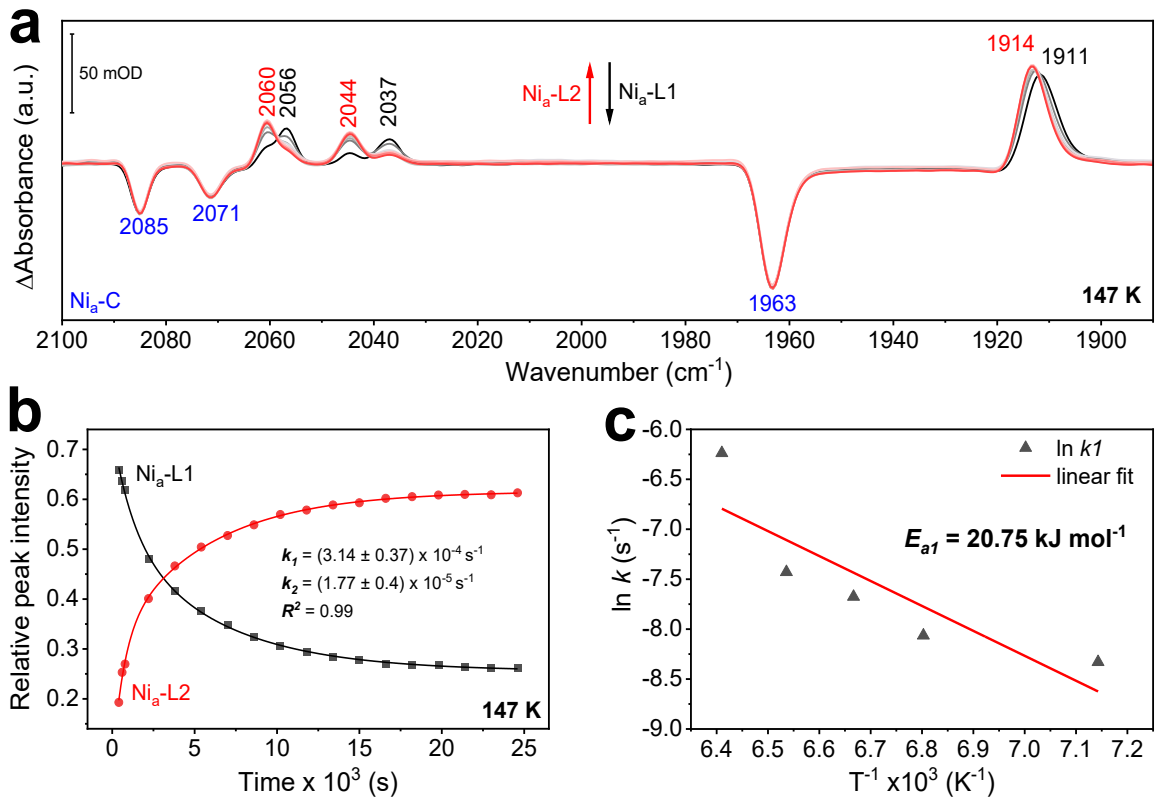

Figure 5. Kinetic study of the Ni_a-L1 to Ni_a-L2 conversion. (**a**) Representative (light-*minus*-dark) IR difference spectra of the H_2-reduced *Cn*RH at 147 K. The positive bands in the black (difference) spectrum represent the Ni_a-L1 species populated upon illumination of *Cn*RH in the Ni_a-C state for 0.5 h with an LED array (460 nm). The positive bands in the red spectrum are related to the Ni_a-L2 species formed keeping the Ni_a-L1 species in the dark for ca 7h. The grey spectra show the time dependent Ni_a-L1 to Ni_a-L2 conversion. The single beam spectrum of Ni_a-C recorded in the dark before illumination was used as reference and consequently contributes to the negative bands (blue labels). (**b**) Kinetic profile of the Ni_a-L1 to Ni_a-L2 conversion at 147 K. The relative peak intensities of Ni_a-L1 (absorption bands at 1911 (ν_{CO}), 2037 (ν_{CN}) and 2056 cm^{-1} (ν_{CN}) and Ni_a-L2 (1914 (ν_{CO}), 2044 (ν_{CN}) and 2060 cm^{-1} (ν_{CN}) were plotted against time (same color code as in (**a**)). The fitted curves exhibit bi-exponential kinetics (see **Fig. S10** for data at other temperatures)**.** Data related to the intensity decrease of Ni_a-L1 over time were used for the kinetic analysis. (**c**) Temperature dependence of the rate constants k (in s^{-1}) of the Ni_a-L1 to Ni_a-L2 conversion, resulting in an energy barrier of 20.7 kJ mol^{-1}. E_{a1} refers to the fast process occurring during the Ni_a-L1 to Ni_a-L2 conversion. The corresponding data and the fitting parameters used to estimate the E_a value for the slow process are shown in **Fig. S10**.

Notably, reduction of the enzyme with D_2 had little to no effect on the rate of the Ni_a-L1 to Ni_a-L2 conversion as the corresponding time constant was only slightly higher (ca 20 %) than that for the enzyme samples prepared with H_2/H_2O (**Fig. S12a**, **b**). In contrast, the rate of the Ni_a-L2 to Ni_a-C backreaction is about three times slower for *Cn*RH prepared with D_2/D_2O (**Fig. S12c**, **d**), consistent with the larger kinetic isotope effects observed for *Dv*MF and *Pf*SH1 hydrogenases.[32,51]

In addition to the hydride rebinding in the Ni_a-L2 to Ni_a-C backreaction, a primary isotope effect has been also observed for the (electron-coupled) deprotonation of a Ni-bound cysteine of *Pf*SH1 during transition from Ni_a-L1/2 to Ni_a-S (30–40 kJ mol^{-1}).[21,52] In contrast, our data indicate that the Ni_a-L1 to Ni_a-L2 conversion does not involve the formation or breaking of a covalent bond with a protonated/deuterated atom.

Considering the small shift between the ν_{CO} modes of the Ni_a-L1/2 species in *Cn*RH ($\Delta\nu$ = 3 cm^{-1}) and *Pf*SH1 ($\Delta\nu$ = 5 cm^{-1}),[32] as well as the sharp ν_{SH} and ν_{SD} absorptions in the Ni_a-L2 state of *Cn*RH, we propose that the estimated energy barrier of ca 20.7 kJ mol^{-1} is related to protein rearrangements that lead to the formation of a H-bond involving the protonated Cys479 in the Ni_a-L2 intermediate. Cysteines are commonly found as H-bond donors (Cys-S–H---X), and DFT studies have shown that relatively strong H-bonds are expected between protonated cysteines and carboxylate side groups (Cys-S–H---$^{-}O_2C$-R).[53] A potential candidate is the conserved Glu13 located in proximity to the proposed protonable Ni-bound cysteine (**Fig. 4c**).[22,52,54,55] This residue has been shown to be part of the proton transfer pathway in various [NiFe]-hydrogenases and, its replacement either abolished or drastically reduced H_2 oxidation activity.[52,54,55] For the corresponding Glu17 in *Pf*SH1, time-resolved IR data revealed that it acts as the proton acceptor for the conversion of Ni_a-S to Ni_a-C, and it has been proposed to stabilize one of the Ni_a-L species via H-bonding.[17] However, corresponding experimental evidence for this assumption has not yet been provided. Based on the homogenous enrichment of the Ni_a-L1 and Ni_a-L2 states in *Cn*RH, we identified specific spectral changes caused by amino acid residues in proximity of the active site by analyzing Ni_a-L1-*minus*-Ni_a-L2 difference spectra.

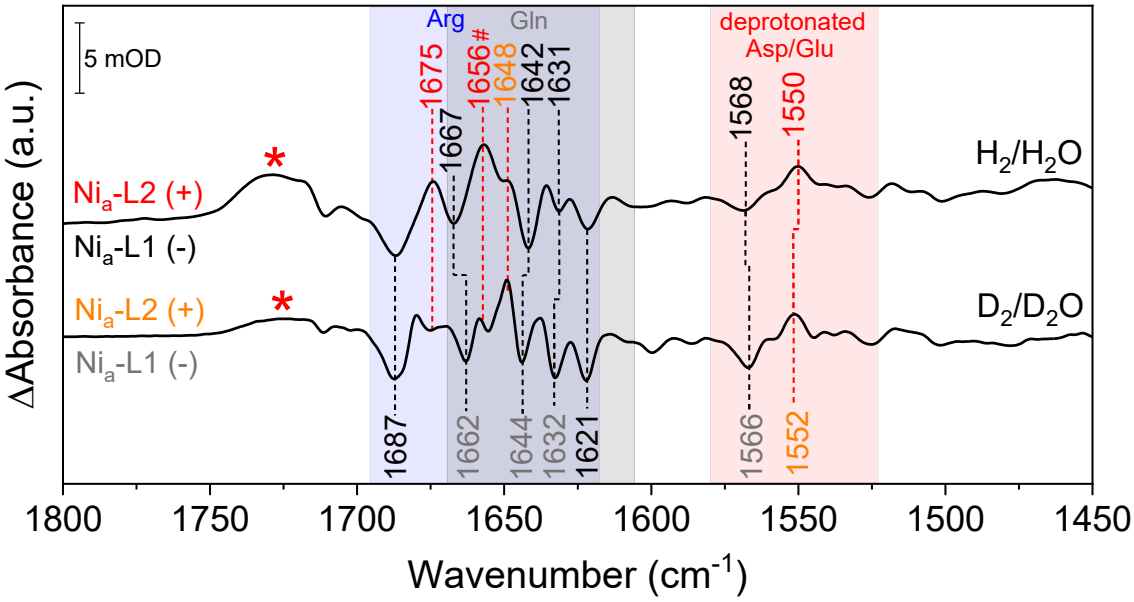

Figure 6. Frequency regime between 1800 and 1450 cm^{-1} of the Ni$_a$-L1-*minus*-Ni$_a$-L2 IR difference spectra of *Cn*RH including spectral contributions of various amino acid residues. The red and blue traces represent the difference spectra of *Cn*RH reduced with H_2 (in H_2O) and with D_2 (in D_2O), respectively. The differently colored bars indicate the spectral regions dominated by vibrational modes from arginine, glutamine, and deprotonated aspartate/glutamate residues. The observed bands most probably originate from residues that form H-bonds to the active site, namely Arg411, Glu13, and Gln67. The color code is identical to that in **Fig. 3d**. The band marked with # most likely originates from OH bending vibrations of water molecule(s) in the proximity of the active site in the Ni$_a$-L2 state, which is supported by its disappearance in the spectra of D_2/D_2O-prepared enzymes. The broad band around 1700-1730 cm^{-1} (*) is an artifact due to slight temperature fluctuations over time.

Fig. 6 shows a clear negative band at 1568 cm^{-1} in the Ni$_a$-L1 state, which is replaced by a positive band at 1550 cm^{-1} in the Ni$_a$-L2 state. These bands fall within the spectral range of deprotonated glutamate residues, and the observed downshift by Δν = -18 cm^{-1} suggests a significantly stronger H-bonding of this particular residue in the Ni$_a$-L2 state.[37] The AlphaFill model of *Cn*RH shows that the Glu13 is located at H-bonding distance (*ca* 3 Å) from Cys479 (**Fig. 4c**), which is consistent with the position of the corresponding glutamate residues in several experimentally derived [NiFe]-hydrogenase structures. Taking into account the sharp ν_{SH} and ν_{SD} absorptions, and the fact that the Ni$_a$-L2 state is more stable than the Ni$_a$-L1 state by ca 20.7 kJ mol^{-1}, we propose that the 1550 cm^{-1} band originates from the carboxylate stretching mode (ν_{COO^-}) of deprotonated Glu13 that forms an H-bond with the protonated Cys479 in the Ni$_a$-L2 intermediate (**Fig. 7**).

Additional signals are evident in the Ni$_a$-L1-*minus*-Ni$_a$-L2 difference spectra, indicating that other amino acid residues are either involved or affected by the Ni$_a$-L1 to Ni$_a$-L2 conversion. Significant negative band contributions for Ni$_a$-L1 were observed at 1687, 1667, 1642, and 1621 cm^{-1} (**Fig. 6**) while positive bands for Ni$_a$-L2 were detectable at 1675, 1656 and 1648 cm^{-1}, respectively. This corresponds

to the spectral range characteristic for arginine, asparagine and glutamine residues.[36,37] Arg411 and Gln67 are located in proximity of the NiFe site of *Cn*RH (**Fig. 4a**)[46,50], and most probably their rearrangements during the Ni_a-L1 to Ni_a-L2 conversion lead to the observed spectral changes.

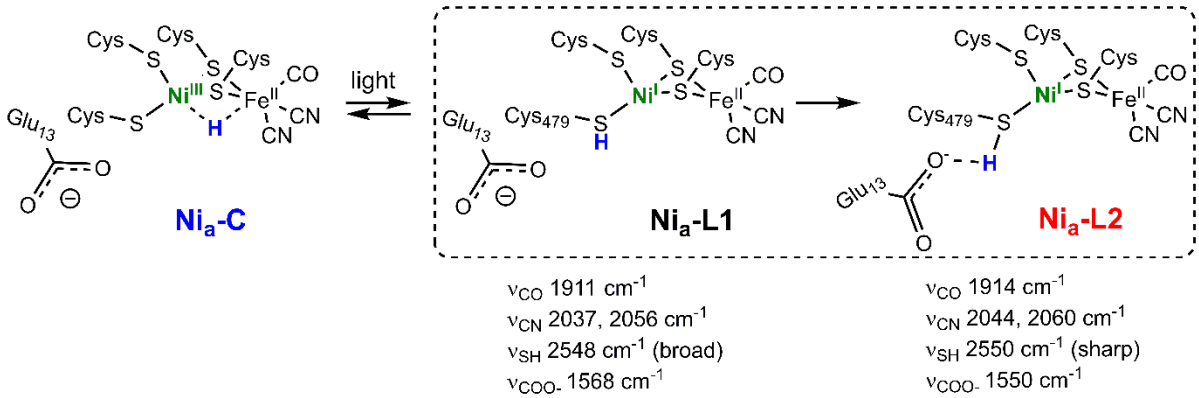

Figure 7. Proposed mechanism for the sequential conversion of Ni_a-C state to the Ni_a-L1 and Ni_a-L2 states. The corresponding wavenumbers of the observed stretching vibrations of the CO and CN^- ligands, the S–H of protonated Cys479, and the COO^- groups of deprotonated Glu13 are listed below the panel frame containing the Ni_a-L1 and Ni_a-L2 structures.

The Arg411 in RH belongs to the invariant amino acid residues in [NiFe]-hydrogenases,[56] and it has been shown to participate in one or two H-bonds (via the guanidinium and peptide NH groups) with a CN ligand.[57] Notably, different research groups have assigned a role to this residue in catalysis. The Armstrong group proposed that the corresponding Arg509 in *Ec*Hyd1 (**Fig. S1**), together with the active site metal atoms, acts as a frustrated Lewis pair that mediates the first step of H_2 activation.[58] In a more recent report from the Dyer group, it was shown that replacement of the corresponding Arg in *Pf*SH1 (Arg355, **Fig. S1**) by lysine impairs the tautomeric equilibrium of the Ni_a-C⇄Ni_a-L interconversion and prevents hydride binding in the active site.[30] Gln67 has been shown to be located at H-bonding distance from one of the bridging cysteines of the active site in the *Cn*RH.[50] Accordingly, the AlphaFill model localizes residues Gln67 and Arg411 near the bridging Cys482 (**Fig. 4d**) and one of the CN ligands (**Fig. 4b**), respectively.

Significantly, the observed IR bands in the Ni_a-L1-*minus*-Ni_a-L2 difference spectra are almost H/D insensitive. In fact, arginine (pK_a ≈ 13.8) and glutamine side groups indeed do not readily exchange protons with deuterons. A clear exception in the H/D IR difference spectra is the positive band at 1656 cm^{-1}, which completely disappears upon incubation of the *Cn*RH with D_2O (**Fig. 6**, bottom trace) whereupon we attribute the respective absorption to one or more water molecules in vicinity of the NiFe center.

Furthermore, previous data on *D. fructosivorans* [NiFe]-hydrogenase showed that alterations of residues involved in H-bonding with the active site CN ligands result in larger shifts for the ν_{CN} bands whereas the ν_{CO} band remain almost unaffected.[59] Such effect is rarely observed in [NiFe]-hydrogenases, since the ν_{CO} band is usually more sensitive to redox and structural changes of the

active site, being in trans position to the substrate-binding site of the catalytic center.[60] Strikingly, the ν_{CO} band (**Fig. 3a**) exhibits a smaller spectral shift ($\Delta\nu_{CO} \approx 3$ cm^{-1}) in the Ni_a-L1 to Ni_a-L2 conversion than the symmetric ($\Delta\nu_{CN} = 7$ cm^{-1}) and antisymmetric ($\Delta\nu_{CN} = 5$ cm^{-1}) stretching vibrations of the CN ligands. Therefore, we hypothesize that the larger spectral shift of the ν_{CN} bands during the Ni_a-L1 to Ni_a-L2 transition results from conformational changes of residues involved in H-bonding with CN ligand(s). This and the observation of positive and negative bands in the IR difference spectra within the spectral range characteristic for arginine led us to conclude that Arg411 undergoes conformational changes during the Ni_a-L1 to Ni_a-L2 transition.

Conclusions

Based on the presented spectroscopic data on the RH from *C. necator*, we draw the following conclusions on the Ni_a-L1 and Ni_a-L2 intermediates. Upon photolysis of the bridging hydride of the Ni_a-C state, the two resulting Ni_a-L1 and Ni_a-L2 intermediates host a protonated thiolate at a Ni-bound cysteine (Cys479 in *Cn*RH, **Fig. 7**). In the Ni_a-L2 state, the corresponding proton forms an H-bond with the deprotonated carboxylic group of a conserved glutamate residue (Glu13 in *Cn*RH). The two Ni_a-L species are neither in a temperature- nor in a pH-dependent equilibrium. Ni_a-L1 represents a metastable species and spontaneously converts to the Ni_a-L2 intermediate with an activation energy barrier of approximately E_a = 21 kJ mol^{-1}. Due to the small E_a value and the fast turnover of hydrogenases, a homogeneous enrichment of this intermediate and its spectroscopic characterization has not been possible so far. The Ni_a-C to Ni_a-L1 and Ni_a-L1 to Ni_a-L2 conversions are associated with structural changes in the 2nd coordination sphere of the active site, which can be seen in the spectral regime between 1750 and 1450 cm^{-1} of the IR difference spectra. We detected absorptions indicative for structural rearrangements of the Arg411 (H-bonded to a CN ligand), Glu13 (H-bonded to the protonated Cys479), and Gln67 (H-bonded to the bridging Cys482) residues (**Fig. 4**), as well as potentially present water molecule(s). Contrary to recent findings on the O_2-sensitive *Dv*MF hydrogenase, Glu13 of *Cn*RH remains deprotonated in the intermediates Ni_a-C, Ni_a-L1, and Ni_a-L2, as tentatively proposed for the O_2-tolerant *Pf*SH1 hydrogenase. Thus, reaction mechanisms among [NiFe]-hydrogenases might be slightly different. Our results not only provide novel insights into the sophisticated mechanism of H_2 activation in [NiFe]-hydrogenases, but also deciphered the often-overlooked contribution of the protein scaffold to fine-tune proton and electron dynamics, which is of general importance for structure/function studies of (metallo)enzymes operating with effective proton/electron transfer mechanisms. In this context, our results also have implications for the design of effective synthetic complexes and artificial metallopeptides (see, e.g., ref [61]) featuring hydrogenase-like reactivity.

Experimental methods

Bacterial strains cultivation and protein preparation

Recombinant *C. necator* strains carrying plasmids for overproduction of RH was cultivated in a basic mineral medium containing fructose and glycerol as the carbon and energy sources.[62] When the bacterial cultures reached an optical density at 436 nm of 11-13, the cells were harvested by centrifugation (11,500 x *g*, 4 °C, 15 min), and the cell pellet was flash frozen in liquid nitrogen and stored at –80 °C until further use. RH of *C. necator* was purified as described before.[62] Cell pellets of recombinant strains were resuspended in lysis buffer (5 mL of buffer per g wet cell paste) consisting of 50 mM Tris-HCl, pH 8.0, 150 mM NaCl, protease inhibitor cocktail (cOmplete EDTA-free, Roche) and DNase I (Roche). The cells were subsequently disrupted in a French pressure cell (G. Heinemann Ultraschall and Labortechnik, Schwäbisch Gmünd, Germany) at 125 MPa. Crude extracts were ultracentrifuged for 40 min at 100,000 x *g* and 4 °C, and the resulting soluble extract was loaded onto a Strep-Tactin® high-capacity column (IBA, Göttingen, Germany). The column was washed with ten bed volumes of washing buffer (50 mM Tris-HCl, pH 8.0, 150 mM NaCl), and the proteins were eluted with 4 bed volumes of washing buffer containing 3 mM D-desthiobiotin. The eluted proteins were concentrated by ultrafiltration (4,000 x *g*, 4 °C) using Amicon Ultracel concentrators (Millipore) with a 50 kDa cut-off. The resulting protein solution was diluted 20-fold with washing buffer and again re-concentrated by ultrafiltration. The final concentrate was flash-frozen and stored in liquid nitrogen. The protein concentration was determined using a Pierce BCA Protein Assay kit (Thermo Scientific) using bovine serum albumin (BSA) as standard. The protein purity was assessed by SDS-PAGE.

Calculation of the activation energy

The CO/CN absorption bands of Ni_a-L1, Ni_a-L2 and Ni_a-C states at different temperatures have been integrated and their kinetic profiles were evaluated using the OriginPro 2021 software. The rate constants of the Ni_a-L1 to Ni_a-L2 and Ni_a-L2 to Ni_a-C exhibited a clear temperature dependence; therefore, both processes are associated with a distinct activation energy barrier (E_a).

The fit parameters are summarized in **Table S3** for the Ni_a-L1 → Ni_a-L2 conversion and **Table S4** for the Ni_a-L2 → Ni_a-C backreaction. The temperature dependence of the obtained rate constants (*k*) follows the Arrhenius equation $\ln(k) = \ln(A) - (E_a/RT)$, in which A is the pre-exponential factor in s^{-1}, E_a is the activation energy in kJ mol^{-1}, *R* is the universal gas constant and T is the temperature in K.

3D-structure prediction

The model for the holo RH large subunit was downloaded from the AlphaFold protein structure database[47] (UniProt Q79IP6, **Fig. S9**) and fed to the web-based user interface AlphaFill (https://alphafill.eu/), enabling to transplant small molecules and ions from experimentally determined structures to predict protein models with their active sites or other cofactors.[48] Among the provided models, we considered exclusively structures with the highest sequence identities (between 30 and 40%). The transplanted hydrogenase active site was optimized using the AlphaFill web-interface to have a TCS (transplant clash score) below 0.29, which is considered high confidence.[48]

IR spectroscopy

For IR measurements the *Cn*RH sample was prepared in 50 mM Tris-HCl (pH 8.0, at 4 °C) buffer solution containing 150 mM NaCl and 25% glycerol and concentrated to ca 1.2 mM. The glycerol ensures a transparent glass in the frozen state. The sample was subsequently reduced by exposure to humidified 100% H_2 or D_2 gas in an anaerobic chamber operating with forming gas (95% N_2, 5% H_2). The samples were transferred into a gas-tight micro-cuvette for cryogenic measurements consisting of two CaF_2 windows with an optical pathlength of 4 µm. The cell was then transferred into a homemade liquid-nitrogen cryostat mounted in the sample compartment of a Bruker Tensor 27 FTIR spectrometer equipped with a liquid-nitrogen cooled mercury cadmium telluride (MCT) detector. The Bruker OPUS software 7.8 was used to acquire and analyze the data. Spectra with a resolution of 2 cm^{-1} were recorded by averaging 200 scans. The cell compartment was purged with dried air. A buffer spectrum was used as reference to calculate the corresponding absorbance spectra.

Absorbance spectra were calculated from averaged single channel spectra of the sample using a buffer spectrum as reference. Light-*minus*-dark spectra were calculated accordingly with the corresponding dark single spectra as reference.

EPR

Protein solutions of *Cn*RH with a volume of 100 µL in a concentration range of 0.2-0.3 mM were transferred into quartz EPR tubes (4 mm diameter), frozen in cold ethanol (193 K) and stored in liquid nitrogen for further analysis. EPR samples were illuminated during the experiments using the focused light of a collimated 455-nm LED. A Bruker EMXplus spectrometer combined with an ER 4122 SHQE resonator, an Oxford EPR 900 helium flow cryostat and an Oxford ITC4 temperature controller was used for the EPR experiments. Baseline correction of the experimental spectra was done by subtracting a spectrum of buffer solution measured with the same experimental parameters. Broad background fluctuations were additionally corrected by using a polynomial or spline function. If not otherwise noted, the following experimental parameters were used: 1 mW microwave power, 9.29

GHz microwave frequency, 10 G modulation amplitude, and 100 kHz modulation frequency. Numerical simulation of the EPR spectra was conducted using the Matlab toolbox Easyspin 5.2.25.[63]

Data availability

The authors declare that the data supporting the findings of this study are available within the article and the Supplementary Information.

Notes

The authors declare no competing financial interest.

ACKNOWLEDGMENTS

This work was funded by the Deutsche Forschungsgemeinschaft (DFG, German Research Foundation) under Germany's Excellence Strategy-EXC 2008-390540038 ("Unifying Systems in Catalysis-UniSysCat").

ASSOCIATED CONTENT

The Supporting Information contains supporting figures, tables, and references.

AUTHOR INFORMATION

Corresponding Authors

Ingo Zebger – Institut für Chemie, Sekr. PC14, Technische Universität Berlin, D-10623 Berlin, Germany; orcid.org/ 0000-0002-6354-3585; Email: ingo.zebger@tu-berlin.de

Giorgio Caserta – Institut für Chemie, Sekr. PC14, Technische Universität Berlin, D-10623 Berlin, Germany; orcid.org/0000-0003-0986-3059; Email: giorgio.caserta@tu-berlin.de

Authors

Armel F. T. Waffo – Institut für Chemie, Sekr. PC14, Technische Universität Berlin, D-10623 Berlin, Germany; orcid.org/0000-0003-4021-1438

Christian Lorent – Institut für Chemie, Sekr. PC14, Technische Universität Berlin, D-10623 Berlin, Germany; orcid.org/0000-0001-9057-4523

Sagie Katz – Institut für Chemie, Sekr. PC14, Technische Universität Berlin, D-10623 Berlin, Germany; orcid.org/0000-0001-8526-183X

Janna Schoknecht – Institut für Chemie, Sekr. PC14, Technische Universität Berlin, D-10623 Berlin, Germany; orcid.org/0000-0002-2896-8174;

Oliver Lenz – Institut für Chemie, Sekr. PC14, Technische Universität Berlin, D-10623 Berlin, Germany; orcid.org/0000-0003-4550-5128;

References:

(1) Shafaat, H. S.; Rüdiger, O.; Ogata, H.; Lubitz, W. [NiFe] Hydrogenases: A Common Active Site for Hydrogen Metabolism under Diverse Conditions. *Biochim. Biophys. Acta BBA - Bioenerg.* **2013**, *1827* (8–9), 986–1002. https://doi.org/10.1016/j.bbabio.2013.01.015.

(2) Lubitz, W.; Ogata, H.; Rüdiger, O.; Reijerse, E. Hydrogenases. *Chem. Rev.* **2014**, *114* (8), 4081–4148. https://doi.org/10.1021/cr4005814.

(3) Caserta, G.; Zuccarello, L.; Barbosa, C.; Silveira, C. M.; Moe, E.; Katz, S.; Hildebrandt, P.; Zebger, I.; Todorovic, S. Unusual Structures and Unknown Roles of FeS Clusters in Metalloenzymes Seen from a Resonance Raman Spectroscopic Perspective. *Coord. Chem. Rev.* **2022**, *452*, 214287. https://doi.org/10.1016/j.ccr.2021.214287.

(4) Lacasse, M. J.; Zamble, D. B. [NiFe]-Hydrogenase Maturation. *Biochemistry* **2016**, *55* (12), 1689–1701. https://doi.org/10.1021/acs.biochem.5b01328.

(5) Caserta, G.; Hartmann, S.; Van Stappen, C.; Karafoulidi-Retsou, C.; Lorent, C.; Yelin, S.; Keck, M.; Schoknecht, J.; Sergueev, I.; Yoda, Y.; Hildebrandt, P.; Limberg, C.; DeBeer, S.; Zebger, I.; Frielingsdorf, S.; Lenz, O. Stepwise Assembly of the Active Site of [NiFe]-Hydrogenase. *Nat. Chem. Biol.* **2023**. https://doi.org/10.1038/s41589-022-01226-w.

(6) Pandelia, M.-E.; Ogata, H.; Lubitz, W. Intermediates in the Catalytic Cycle of [NiFe] Hydrogenase: Functional Spectroscopy of the Active Site. *ChemPhysChem* **2010**, *11* (6), 1127–1140. https://doi.org/10.1002/cphc.200900950.

(7) Ash, P. A.; Hidalgo, R.; Vincent, K. A. Proton Transfer in the Catalytic Cycle of [NiFe] Hydrogenases: Insight from Vibrational Spectroscopy. *ACS Catal.* **2017**, *7* (4), 2471–2485. https://doi.org/10.1021/acscatal.6b03182.

(8) Tai, H.; Hirota, S.; Stripp, S. T. Proton Transfer Mechanisms in Bimetallic Hydrogenases. *Acc. Chem. Res.* **2021**, *54* (1), 232–241. https://doi.org/10.1021/acs.accounts.0c00651.

(9) Stripp, S. T.; Duffus, B. R.; Fourmond, V.; Léger, C.; Leimkühler, S.; Hirota, S.; Hu, Y.; Jasniewski, A.; Ogata, H.; Ribbe, M. W. Second and Outer Coordination Sphere Effects in Nitrogenase, Hydrogenase, Formate Dehydrogenase, and CO Dehydrogenase. *Chem. Rev.* **2022**, *122* (14), 11900–11973. https://doi.org/10.1021/acs.chemrev.1c00914.

(10) Brecht, M.; van Gastel, M.; Buhrke, T.; Friedrich, B.; Lubitz, W. Direct Detection of a Hydrogen Ligand in the [NiFe] Center of the Regulatory H_2-Sensing Hydrogenase from *Ralstonia e Utropha* in Its Reduced State by HYSCORE and ENDOR Spectroscopy. *J. Am. Chem. Soc.* **2003**, *125* (43), 13075–13083. https://doi.org/10.1021/ja036624x.

(11) Caserta, G.; Lorent, C.; Pelmenschikov, V.; Schoknecht, J.; Yoda, Y.; Hildebrandt, P.; Cramer, S. P.; Zebger, I.; Lenz, O. *In Vitro* Assembly as a Tool to Investigate Catalytic Intermediates of [NiFe]-Hydrogenase. *ACS Catal.* **2020**, *10* (23), 13890–13894. https://doi.org/10.1021/acscatal.0c04079.

(12) Horch, M.; Schoknecht, J.; Mroginski, M. A.; Lenz, O.; Hildebrandt, P.; Zebger, I. Resonance Raman Spectroscopy on [NiFe] Hydrogenase Provides Structural Insights into Catalytic Intermediates and Reactions. *J. Am. Chem. Soc.* **2014**, *136* (28), 9870–9873. https://doi.org/10.1021/ja505119q.

(13) Lorent, C.; Pelmenschikov, V.; Frielingsdorf, S.; Schoknecht, J.; Caserta, G.; Yoda, Y.; Wang, H.; Tamasaku, K.; Lenz, O.; Cramer, S. P.; Horch, M.; Lauterbach, L.; Zebger, I. Exploring Structure and Function of Redox Intermediates in [NiFe]-Hydrogenases by an Advanced Experimental Approach for Solvated, Lyophilized and Crystallized Metalloenzymes. *Angew. Chem. Int. Ed.* **2021**, *60* (29), 15854–15862. https://doi.org/10.1002/anie.202100451.

(14) Roncaroli, F.; Bill, E.; Friedrich, B.; Lenz, O.; Lubitz, W.; Pandelia, M.-E. Cofactor Composition and Function of a H_2-Sensing Regulatory Hydrogenase as Revealed by Mössbauer and EPR Spectroscopy. *Chem. Sci.* **2015**, *6* (8), 4495–4507. https://doi.org/10.1039/C5SC01560J.

(15) Ash, P. A.; Liu, J.; Coutard, N.; Heidary, N.; Horch, M.; Gudim, I.; Simler, T.; Zebger, I.; Lenz, O.; Vincent, K. A. Electrochemical and Infrared Spectroscopic Studies Provide Insight into Reactions of the NiFe Regulatory Hydrogenase from *Ralstonia Eutropha* with O_2 and CO. *J. Phys. Chem. B* **2015**, *119* (43), 13807–13815. https://doi.org/10.1021/acs.jpcb.5b04164.
(16) Tai, H.; Higuchi, Y.; Hirota, S. Comprehensive Reaction Mechanisms at and near the Ni–Fe Active Sites of [NiFe] Hydrogenases. *Dalton Trans.* **2018**, *47* (13), 4408–4423. https://doi.org/10.1039/C7DT04910B.
(17) Greene, B. L.; Vansuch, G. E.; Chica, B. C.; Adams, M. W. W.; Dyer, R. B. Applications of Photogating and Time Resolved Spectroscopy to Mechanistic Studies of Hydrogenases. *Acc. Chem. Res.* **2017**, *50* (11), 2718–2726. https://doi.org/10.1021/acs.accounts.7b00356.
(18) van der Zwaan, J. W.; Albracht, S. P. J.; Fontijn, R. D.; Slater, E. C. Monovalent Nickel in Hydrogenase from *Chromatium Vinosum*: Light Sensitivity and Evidence for Direct Interaction with Hydrogen. *FEBS Lett.* **1985**, *179* (2), 271–277. https://doi.org/10.1016/0014-5793(85)80533-0.
(19) Tai, H.; Nishikawa, K.; Suzuki, M.; Higuchi, Y.; Hirota, S. Control of the Transition between Ni-C and Ni-SI $_a$ States by the Redox State of the Proximal Fe□S Cluster in the Catalytic Cycle of [NiFe] Hydrogenase. *Angew. Chem. Int. Ed.* **2014**, *53* (50), 13817–13820. https://doi.org/10.1002/anie.201408552.
(20) Hidalgo, R.; Ash, P. A.; Healy, A. J.; Vincent, K. A. Infrared Spectroscopy During Electrocatalytic Turnover Reveals the Ni-L Active Site State During H_2 Oxidation by a NiFe Hydrogenase. *Angew. Chem. Int. Ed.* **2015**, *54* (24), 7110–7113. https://doi.org/10.1002/anie.201502338.
(21) Greene, B. L.; Wu, C.-H.; Vansuch, G. E.; Adams, M. W. W.; Dyer, R. B. Proton Inventory and Dynamics in the Ni_a-S to Ni_a-C Transition of a [NiFe] Hydrogenase. *Biochemistry* **2016**, *55* (12), 1813–1825. https://doi.org/10.1021/acs.biochem.5b01348.
(22) Tai, H.; Nishikawa, K.; Higuchi, Y.; Mao, Z.; Hirota, S. Cysteine SH and Glutamate COOH Contributions to [NiFe] Hydrogenase Proton Transfer Revealed by Highly Sensitive FTIR Spectroscopy. *Angew. Chem. Int. Ed.* **2019**, *58* (38), 13285–13290. https://doi.org/10.1002/anie.201904472.
(23) Ogata, H.; Nishikawa, K.; Lubitz, W. Hydrogens Detected by Subatomic Resolution Protein Crystallography in a [NiFe] Hydrogenase. *Nature* **2015**, *520* (7548), 571–574. https://doi.org/10.1038/nature14110.
(24) Ogata, H.; Krämer, T.; Wang, H.; Schilter, D.; Pelmenschikov, V.; van Gastel, M.; Neese, F.; Rauchfuss, T. B.; Gee, L. B.; Scott, A. D.; Yoda, Y.; Tanaka, Y.; Lubitz, W.; Cramer, S. P. Hydride Bridge in [NiFe]-Hydrogenase Observed by Nuclear Resonance Vibrational Spectroscopy. *Nat. Commun.* **2015**, *6* (1), 7890. https://doi.org/10.1038/ncomms8890.
(25) Ash, P. A.; Kendall-Price, S. E. T.; Evans, R. M.; Carr, S. B.; Brasnett, A. R.; Morra, S.; Rowbotham, J. S.; Hidalgo, R.; Healy, A. J.; Cinque, G.; Frogley, M. D.; Armstrong, F. A.; Vincent, K. A. The Crystalline State as a Dynamic System: IR Microspectroscopy under Electrochemical Control for a [NiFe] Hydrogenase. *Chem. Sci.* **2021**, *12* (39), 12959–12970. https://doi.org/10.1039/D1SC01734A.
(26) Ash, P. A.; Kendall-Price, S. E. T.; Vincent, K. A. Unifying Activity, Structure, and Spectroscopy of [NiFe] Hydrogenases: Combining Techniques To Clarify Mechanistic Understanding. *Acc. Chem. Res.* **2019**, *52* (11), 3120–3131. https://doi.org/10.1021/acs.accounts.9b00293.
(27) Pierik, A. J.; Schmelz, M.; Lenz, O.; Friedrich, B.; Albracht, S. P. J. Characterization of the Active Site of a Hydrogen Sensor from *Alcaligenes Eutrophus*. *FEBS Lett.* **1998**, *438* (3), 231–235. https://doi.org/10.1016/S0014-5793(98)01306-4.
(28) Caserta, G.; Lorent, C.; Ciaccafava, A.; Keck, M.; Breglia, R.; Greco, C.; Limberg, C.; Hildebrandt, P.; Cramer, S. P.; Zebger, I.; Lenz, O. The Large Subunit of the Regulatory [NiFe]-Hydrogenase from *Ralstonia Eutropha* – a Minimal Hydrogenase? *Chem. Sci.* **2020**, *11* (21), 5453–5465. https://doi.org/10.1039/D0SC01369B.

(29) Caserta, G.; Pelmenschikov, V.; Lorent, C.; Tadjoung Waffo, A. F.; Katz, S.; Lauterbach, L.; Schoknecht, J.; Wang, H.; Yoda, Y.; Tamasaku, K.; Kaupp, M.; Hildebrandt, P.; Lenz, O.; Cramer, S. P.; Zebger, I. Hydroxy-Bridged Resting States of a [NiFe]-Hydrogenase Unraveled by Cryogenic Vibrational Spectroscopy and DFT Computations. *Chem. Sci.* **2021**, *12* (6), 2189–2197. https://doi.org/10.1039/D0SC05022A.
(30) Vansuch, G. E.; Wu, C.-H.; Haja, D. K.; Blair, S. A.; Chica, B.; Johnson, M. K.; Adams, M. W. W.; Dyer, R. B. Metal–Ligand Cooperativity in the Soluble Hydrogenase-1 from *Pyrococcus Furiosus*. *Chem. Sci.* **2020**, *11* (32), 8572–8581. https://doi.org/10.1039/D0SC00628A.
(31) Murphy, B. J.; Hidalgo, R.; Roessler, M. M.; Evans, R. M.; Ash, P. A.; Myers, W. K.; Vincent, K. A.; Armstrong, F. A. Discovery of Dark PH-Dependent H^+ Migration in a [NiFe]-Hydrogenase and Its Mechanistic Relevance: Mobilizing the Hydrido Ligand of the Ni-C Intermediate. *J. Am. Chem. Soc.* **2015**, *137* (26), 8484–8489. https://doi.org/10.1021/jacs.5b03182.
(32) Greene, B. L.; Wu, C.-H.; McTernan, P. M.; Adams, M. W. W.; Dyer, R. B. Proton-Coupled Electron Transfer Dynamics in the Catalytic Mechanism of a [NiFe]-Hydrogenase. *J. Am. Chem. Soc.* **2015**, *137* (13), 4558–4566. https://doi.org/10.1021/jacs.5b01791.
(33) Ouattara, A. S.; Patel, B. K. C.; Cayol, J.-L.; Cuzin, N.; Traore, A. S.; Garcia, J.-L. NOTE: Isolation and Characterization of Desulfovibrio Burkinensis Sp. Nov. from an African Ricefield, and Phylogeny of Desulfovibrio Alcoholivorans. *Int. J. Syst. Evol. Microbiol.* **1999**, *49* (2), 639–643. https://doi.org/10.1099/00207713-49-2-639.
(34) Medina, M.; Claude Hatchikian, E.; Cammack, R. Studies of Light-Induced Nickel EPR Signals in Hydrogenase: Comparison of Enzymes with and without Selenium. *Biochim. Biophys. Acta BBA - Bioenerg.* **1996**, *1275* (3), 227–236. https://doi.org/10.1016/0005-2728(96)00007-2.
(35) Medina, M.; Williams, R.; Cammack, R.; Hatchikian, E. C. Studies of Light-Induced Nickel EPR Signals in Desulfovibrio Gigas Hydrogenase. *J. Chem. Soc. Faraday Trans.* **1994**, *90* (19), 2921. https://doi.org/10.1039/ft9949002921.
(36) Barth, A. Infrared Spectroscopy of Proteins. *Biochim. Biophys. Acta BBA - Bioenerg.* **2007**, *1767* (9), 1073–1101. https://doi.org/10.1016/j.bbabio.2007.06.004.
(37) Lorenz-Fonfria, V. A. Infrared Difference Spectroscopy of Proteins: From Bands to Bonds. *Chem. Rev.* **2020**, *120* (7), 3466–3576. https://doi.org/10.1021/acs.chemrev.9b00449.
(38) Stripp, S. T. In Situ Infrared Spectroscopy for the Analysis of Gas-Processing Metalloenzymes. *ACS Catal.* **2021**, *11* (13), 7845–7862. https://doi.org/10.1021/acscatal.1c00218.
(39) Yang, H.; Yang, S.; Kong, J.; Dong, A.; Yu, S. Obtaining Information about Protein Secondary Structures in Aqueous Solution Using Fourier Transform IR Spectroscopy. *Nat. Protoc.* **2015**, *10* (3), 382–396. https://doi.org/10.1038/nprot.2015.024.
(40) Deniz, E.; Schmidt-Engler, J. M.; Ulrich, K.; Oberle, M.; Wille, G.; Bredenbeck, J. SH—It Happens: S–H Bonds as Intrinsic 2D-IR Labels in Proteins. *J. Chem. Phys.* **2022**, *157* (13), 135102. https://doi.org/10.1063/5.0107057.
(41) Bare, G. H.; Alben, J. O.; Bromberg, P. A. Sulfhydryl Groups in Hemoglobin. New Molecular Probe at the A1β1 Interface Studied by Fourier Transform Infrared Spectroscopy. *Biochemistry* **1975**, *14* (8), 1578–1583. https://doi.org/10.1021/bi00679a005.
(42) Kandori, H.; Kinoshita, N.; Shichida, Y.; Maeda, A.; Needleman, R.; Lanyi, J. K. Cysteine S−H as a Hydrogen-Bonding Probe in Proteins. *J. Am. Chem. Soc.* **1998**, *120* (23), 5828–5829. https://doi.org/10.1021/ja980837i.
(43) Li, H.; Thomas, G. J. Studies of Virus Structure by Raman Spectroscopy. Cysteine Conformation and Sulfhydryl Interactions in Proteins and Viruses. 1. Correlation of the Raman Sulfur-Hydrogen Band with Hydrogen Bonding and Intramolecular Geometry in Model Compounds. *J. Am. Chem. Soc.* **1991**, *113* (2), 456–462. https://doi.org/10.1021/ja00002a012.
(44) Sato, Y.; Nabeno, M.; Iwata, T.; Tokutomi, S.; Sakurai, M.; Kandori, H. Heterogeneous Environment of the S−H Group of Cys966 near the Flavin Chromophore in the LOV2 Domain of *Adiantum* Neochrome1. *Biochemistry* **2007**, *46* (36), 10258–10265. https://doi.org/10.1021/bi701022v.

(45) Bürstel, I.; Hummel, P.; Siebert, E.; Wisitruangsakul, N.; Zebger, I.; Friedrich, B.; Lenz, O. Probing the Origin of the Metabolic Precursor of the CO Ligand in the Catalytic Center of [NiFe] Hydrogenase. *J. Biol. Chem.* **2011**, *286* (52), 44937–44944. https://doi.org/10.1074/jbc.M111.309351.
(46) Kleihues, L.; Lenz, O.; Bernhard, M.; Buhrke, T.; Friedrich, B. The H $_2$ Sensor of *Ralstonia Eutropha* Is a Member of the Subclass of Regulatory [NiFe] Hydrogenases. *J. Bacteriol.* **2000**, *182* (10), 2716–2724. https://doi.org/10.1128/JB.182.10.2716-2724.2000.
(47) Jumper, J.; Evans, R.; Pritzel, A.; Green, T.; Figurnov, M.; Ronneberger, O.; Tunyasuvunakool, K.; Bates, R.; Žídek, A.; Potapenko, A.; Bridgland, A.; Meyer, C.; Kohl, S. A. A.; Ballard, A. J.; Cowie, A.; Romera-Paredes, B.; Nikolov, S.; Jain, R.; Adler, J.; Back, T.; Petersen, S.; Reiman, D.; Clancy, E.; Zielinski, M.; Steinegger, M.; Pacholska, M.; Berghammer, T.; Bodenstein, S.; Silver, D.; Vinyals, O.; Senior, A. W.; Kavukcuoglu, K.; Kohli, P.; Hassabis, D. Highly Accurate Protein Structure Prediction with AlphaFold. *Nature* **2021**, *596* (7873), 583–589. https://doi.org/10.1038/s41586-021-03819-2.
(48) Hekkelman, M. L.; de Vries, I.; Joosten, R. P.; Perrakis, A. AlphaFill: Enriching AlphaFold Models with Ligands and Cofactors. *Nat. Methods* **2022**. https://doi.org/10.1038/s41592-022-01685-y.
(49) Frielingsdorf, S.; Fritsch, J.; Schmidt, A.; Hammer, M.; Löwenstein, J.; Siebert, E.; Pelmenschikov, V.; Jaenicke, T.; Kalms, J.; Rippers, Y.; Lendzian, F.; Zebger, I.; Teutloff, C.; Kaupp, M.; Bittl, R.; Hildebrandt, P.; Friedrich, B.; Lenz, O.; Scheerer, P. Reversible [4Fe-3S] Cluster Morphing in an O2-Tolerant [NiFe] Hydrogenase. *Nat. Chem. Biol.* **2014**, *10* (5), 378–385. https://doi.org/10.1038/nchembio.1500.
(50) Buhrke, T.; Brecht, M.; Lubitz, W.; Friedrich, B. The H2 Sensor of Ralstonia Eutropha: Biochemical and Spectroscopic Analysis of Mutant Proteins Modified at a Conserved Glutamine Residue Close to the [NiFe] Active Site. *JBIC J. Biol. Inorg. Chem.* **2002**, *7* (7–8), 897–908. https://doi.org/10.1007/s00775-002-0379-6.
(51) Kellers, P.; Pandelia, M.-E.; Currell, L. J.; Görner, H.; Lubitz, W. FTIR Study on the Light Sensitivity of the [NiFe] Hydrogenase from Desulfovibrio Vulgaris Miyazaki F: Ni–C to Ni–L Photoconversion, Kinetics of Proton Rebinding and H/D Isotope Effect. *Phys. Chem. Chem. Phys.* **2009**, *11* (39), 8680. https://doi.org/10.1039/b913635e.
(52) Greene, B. L.; Vansuch, G. E.; Wu, C.-H.; Adams, M. W. W.; Dyer, R. B. Glutamate Gated Proton-Coupled Electron Transfer Activity of a [NiFe]-Hydrogenase. *J. Am. Chem. Soc.* **2016**, *138* (39), 13013–13021. https://doi.org/10.1021/jacs.6b07789.
(53) Mazmanian, K.; Sargsyan, K.; Grauffel, C.; Dudev, T.; Lim, C. Preferred Hydrogen-Bonding Partners of Cysteine: Implications for Regulating Cys Functions. *J. Phys. Chem. B* **2016**, *120* (39), 10288–10296. https://doi.org/10.1021/acs.jpcb.6b08109.
(54) Dementin, S.; Burlat, B.; De Lacey, A. L.; Pardo, A.; Adryanczyk-Perrier, G.; Guigliarelli, B.; Fernandez, V. M.; Rousset, M. A Glutamate Is the Essential Proton Transfer Gate during the Catalytic Cycle of the [NiFe] Hydrogenase. *J. Biol. Chem.* **2004**, *279* (11), 10508–10513. https://doi.org/10.1074/jbc.M312716200.
(55) Evans, R. M.; Ash, P. A.; Beaton, S. E.; Brooke, E. J.; Vincent, K. A.; Carr, S. B.; Armstrong, F. A. Mechanistic Exploitation of a Self-Repairing, Blocked Proton Transfer Pathway in an O $_2$ -Tolerant [NiFe]-Hydrogenase. *J. Am. Chem. Soc.* **2018**, *140* (32), 10208–10220. https://doi.org/10.1021/jacs.8b04798.
(56) Albracht, S. P. J. Nickel Hydrogenases: In Search of the Active Site. *Biochim. Biophys. Acta BBA - Bioenerg.* **1994**, *1188* (3), 167–204. https://doi.org/10.1016/0005-2728(94)90036-1.
(57) Escorcia, A. M.; Stein, M. QM/MM Investigation of the Role of a Second Coordination Shell Arginine in [NiFe]-Hydrogenases. *Front. Chem.* **2018**, *6*, 164. https://doi.org/10.3389/fchem.2018.00164.
(58) Evans, R. M.; Brooke, E. J.; Wehlin, S. A. M.; Nomerotskaia, E.; Sargent, F.; Carr, S. B.; Phillips, S. E. V.; Armstrong, F. A. Mechanism of Hydrogen Activation by [NiFe] Hydrogenases. *Nat. Chem. Biol.* **2016**, *12* (1), 46–50. https://doi.org/10.1038/nchembio.1976.

(59) De Lacey, A. L.; Fernandez, V. M.; Rousset, M.; Cavazza, C.; Hatchikian, C. E. Spectroscopic and Kinetic Characterization of Active Site Mutants of Desulfovibrio Fructosovorans Ni-Fe Hydrogenase. *JBIC J. Biol. Inorg. Chem.* **2003**, *8* (1), 129–134. https://doi.org/10.1007/s00775-002-0397-4.

(60) Rippers, Y.; Horch, M.; Hildebrandt, P.; Zebger, I.; Mroginski, M. A. Revealing the Absolute Configuration of the CO and CN ⁻ Ligands at the Active Site of a [NiFe] Hydrogenase. *ChemPhysChem* **2012**, *13* (17), 3852–3856. https://doi.org/10.1002/cphc.201200562.

(61) Malayam Parambath, S.; Williams, A. E.; Hunt, L. A.; Selvan, D.; Hammer, N. I.; Chakraborty, S. A De Novo-Designed Artificial Metallopeptide Hydrogenase: Insights into Photochemical Processes and the Role of Protonated Cys. *ChemSusChem* **2021**, *14* (10), 2237–2246. https://doi.org/10.1002/cssc.202100122.

(62) Lenz, O.; Lauterbach, L.; Frielingsdorf, S. O2-Tolerant [NiFe]-Hydrogenases of Ralstonia Eutropha H16: Physiology, Molecular Biology, Purification, and Biochemical Analysis. In *Methods in Enzymology*; Elsevier, 2018; Vol. 613, pp 117–151. https://doi.org/10.1016/bs.mie.2018.10.008.

(63) Stoll, S.; Schweiger, A. EasySpin, a Comprehensive Software Package for Spectral Simulation and Analysis in EPR. *J. Magn. Reson.* **2006**, *178* (1), 42–55. https://doi.org/10.1016/j.jmr.2005.08.013.

TOC